Dielectric susceptibility model for optical phonons in superlattices

T. Dumelow* and S. R. P. Smith
Department of Physics, University of Essex, Wivenhoe Park, Colchester, Essex CO4 3SQ, United Kingdom
(Received 14 August 1997)

The form of the long-wavelength optic-phonon modes in semiconductor superlattices is described using a dielectric susceptibility model. This model only requires knowledge of the frequencies and eigenvalues for LO and TO modes propagating along the superlattice growth direction z. From these, the principal-axis dielectric susceptibilities $\varepsilon_{zz}(\omega)$ and $\varepsilon_{xx}(\omega)$ can be obtained, and so a full description of the optic phonons is possible for any phonon propagation direction. Calculations of confined LO and TO mode frequencies and displacements are made for GaAs/AlAs superlattices. The susceptibilities and mode displacements are compared using a simple continuum model and a microscopic linear-chain model. The susceptibilities are also used to model nonresonant Raman-scattering spectra, and are shown to give results that are in close agreement with published micro-Raman measurements. [S0163-1829(98)02007-4]

I. INTRODUCTION

The form of the atomic displacements in the optic-phonon modes of superlattices has been the subject of many investigations in recent years. The basic problem is easy to formulate if the phonons propagate along the growth axis (the z axis) normal to the layers of a superlattice such as $(\mathrm{GaAs})_{n_1}(\mathrm{AlAs})_{n_2}$. The optic-phonon bands of adjacent layers do not usually overlap in frequency, and so the atomic displacements in the phonon modes of the combined structure are confined to either one or the other component. Therefore, the displacement at a site j of position z_j within a layer of width d is approximately

$$u_m(z_j) \sim \sin(m\pi z_j/d) \quad \text{for } 0 \leqslant z_j \leqslant d, \tag{1}$$

with m an integer representing the order of the confinement. The associated polarization $P \sim u$, so P is also zero at the boundary of the layer. This form is the same whether the phonon modes are transverse or longitudinal, so the problem is essentially a one-dimensional lattice-dynamical problem.

The first lattice-dynamical calculations of the modes were performed by Kunc and Martin,[1] and followed by many others,[2–8] the later ones also showing that interface disorder or roughness has a significant effect on the phonon frequencies in short-period superlattices. However, as soon as the phonon propagation direction departs from being strictly along the z axis, the situation becomes more complicated because of the coupling between the polarization and the macroscopic electric fields. There are then three categories of model used to describe the phonon modes.

(a) The full lattice-dynamical microscopic model calculations[3,7,9–13] in which the long-range electric interactions are evaluated explicitly, often using Ewald's method.

(b) Continuum models, in which the displacement $u(z)$ is treated as a continuous rather than a discrete variable. Such models started as an extension of the work of Fuchs and Kliewer,[14] and include the hydrodynamic continuum model of Babiker.[15] The types of displacements associated with the continuum model when the wave vector is normal to the z axis were substantially clarified by Huang and Zhu.[16] In order to satisfy both the electrostatic boundary conditions involving the macroscopic fields **D** and **E** and the mechanical boundary conditions involving the displacement **u** (usually assumed to be zero at an interface), there is a mixing of the longitudinal LO optic modes with the transverse (''interface'') modes.[17–21] Continuum models normally assume that the bulk phonon dispersion is quadratic in the wave vector, and so they cannot reliably be applied to very-short-period superlattices, where nonparabolicity is important since the microscopic wave vectors $m\pi/d$ are large and also interface disorder is relatively significant.

(c) Dielectric susceptibility models, in which the long-range Coulomb forces produced by the macroscopic **D** and **E** fields are described by the use of an anisotropic dielectric function $\underline{\underline{\varepsilon}}$. This approach has been the least explored; it was originally described in principle by Chu and co-workers,[9,10] and has been applied in the present context by Dumelow and Smith[22] in order to determine the mode frequencies as a function of propagation direction in the long-wavelength limit.

The dielectric susceptibility model (c) has certain advantages over the two other models. In the long-wavelength limit $q \to 0$ (where **q** is the macroscopic Bloch phonon wave vector), the lattice-dynamical problem needed to be solved only for phonons propagating along the z axis, because propagation along other directions can be obtained from this by exploiting the properties of the dielectric function $\underline{\underline{\varepsilon}}$. Propagation along the z axis is essentially a one-dimensional problem, which can be solved using either a microscopic or a continuum method. The dielectric susceptibility model therefore permits a combination of the microscopic (a) and macroscopic (b) approaches without suffering the difficulty inherent in (a) of doing a full lattice-dynamical calculation at arbitrary propagation direction, nor needing the elaborate detailed treatment of the microscopic boundary conditions necessary to (b).

In this paper, we describe the dielectric susceptibility approach to long-wavelength phonons in superlattices. We show how both a continuum and a microscopic model can be used to describe the dielectric response and to calculate the mode displacements as well as the mode frequencies. We

compare the displacement patterns obtained from these models, and also extend the description so that it gives an account of mode intensities that have been observed in Raman-scattering experiments on short-period superlattices.

II. SUPERLATTICE DIELECTRIC SUSCEPTIBILITY

This paper examines the properties of superlattice phonons from the point of view of the dielectric function $\underline{\underline{\varepsilon}}(\mathbf{q},\omega)$. This is a macroscopic quantity that we will obtain by considering the form of the microscopic fields, and it will help to begin with a discussion of the relationship between the microscopic and macroscopic fields. The superlattice is assumed to be homogeneous in the xy plane but has a periodic structure in the z direction with superlattice cell length L. If the fields have macroscopic wave vector $\mathbf{q}$ and angular frequency ω, all microscopic fields $\boldsymbol{\mathcal{F}}(\mathbf{r},t)$ must have the Bloch form

$$\boldsymbol{\mathcal{F}}(\mathbf{r},t)=\mathbf{F}(z)e^{\mathbf{i}(\mathbf{q}\cdot\mathbf{r}-\omega t)}, \tag{2}$$

where $\mathbf{F}(z)$ is periodic in L, i.e., $\mathbf{F}(z+L)=\mathbf{F}(z)$. The corresponding macroscopic field $\overline{\mathbf{F}}(\mathbf{r},t)$ is obtained by simply averaging $\mathbf{F}(z)$ over the superlattice cell:

$$\overline{\mathbf{F}}(\mathbf{r},t)=\overline{\mathbf{F}}e^{i(\mathbf{q}\cdot\mathbf{r}-\omega t)}, \tag{3}$$

where the macroscopic field amplitude is

$$\overline{\mathbf{F}}=\frac{1}{L}\int_{z}^{z+L}\mathbf{F}(z)dz. \tag{4}$$

This definition of $\overline{\mathbf{F}}$ ensures that so long as the microscopic fields satisfy Maxwell's equations, then so do the macroscopic fields. It is appropriate to use the macroscopic fields $\overline{\mathbf{F}}(\mathbf{r},t)$ so long as one does not wish to probe the system on a length scale as small as the cell length L. The dielectric function $\underline{\underline{\varepsilon}}(\mathbf{q},\omega)$ describes the relationship between the macroscopic fields $\mathbf{D}$ and $\mathbf{E}$: thus,

$$\overline{\mathbf{D}}=\varepsilon_0\underline{\underline{\varepsilon}}(\mathbf{q},\omega)\cdot\overline{\mathbf{E}}.$$

In this paper, we are interested in the long-wavelength limit $\mathbf{q}\rightarrow 0$. The bulk isotropic dielectric function for medium i ($i=1$ or 2) has the form

$$\varepsilon_i(\omega)=\varepsilon_i^{\infty}\frac{\omega_{\mathrm{LO}i}^2-\omega^2}{\omega_{\mathrm{TO}i}^2-\omega^2}, \tag{5}$$

where $\omega_{\mathrm{LO}i}$ and $\omega_{\mathrm{LO}i}$ are the bulk LO and TO frequencies, and ε_i^{∞} the high-frequency dielectric constant. An (001)-grown superlattice behaves as a uniaxial medium, and $\underline{\underline{\varepsilon}}(\mathbf{q},\omega)$ can be represented by its principal components $\varepsilon_{xx}(\omega)=\varepsilon_{yy}(\omega)$ and $\varepsilon_{zz}(\omega)$ (usually written as ε_{xx} and ε_{zz}). The simplest evaluation of ε_{xx} and ε_{zz} uses the bulk slab model in which the superlattice layers are assumed to be sufficiently thick to retain their bulk properties. Then

$$\varepsilon_{xx}=\frac{d_1\varepsilon_1+d_2\varepsilon_2}{d_1+d_2},\quad \varepsilon_{zz}^{-1}=\frac{d_1\varepsilon_1^{-1}+d_2\varepsilon_2^{-1}}{d_1+d_2}, \tag{6}$$

where the two constituent layers have thicknesses d_1 and d_2. The above equations may be simply derived (Agranovich and Kravtsov[23]) using the standard condition that $E_x(z)$ and $D_z(z)$ are continuous at the boundaries of the superlattice layers, and, in the long-wavelength limit, constant within each layer. In the far-infrared region in superlattices without free carriers, $\varepsilon_{xx}(\omega)$ has poles at the TO frequencies of the two superlattice constituents and $\varepsilon_{zz}(\omega)$ has zeros at their LO frequencies.

When the superlattice layers are thin, the phonon response is affected by confinement and the bulk slab model is no longer appropriate. In GaAs/AlAs, the optic-phonon dispersion curves of the two constituents do not overlap, so the optic phonons are confined within the individual layers, forming standing wave patterns within these layers. For propagation in the z direction, both the TO and the LO response of each constituent is split into a number of modes μ, each having a different frequency ω_μ and oscillator strength S_μ. The general form of the dielectric tensor, ignoring damping, is then

$$\varepsilon_{xx}=\varepsilon_{xx}^{\infty}\left[1+\sum_{\mu}\frac{S_{T_\mu}}{\omega_{T\mu}^2-\omega^2}\right],$$

$$\frac{1}{\varepsilon_{zz}}=\frac{1}{\varepsilon_{zz}^{\infty}}\left[1-\sum_{\mu}\frac{S_{L\mu}}{\omega_{L\mu}^2-\omega^2}\right], \tag{7}$$

where $\omega_{T\mu}$ and $\omega_{L\mu}$ are the frequencies of the confined TO and LO modes of index μ, $S_{T\mu}$ and $S_{L\mu}$ are their oscillator strengths, and $\varepsilon_{xx}^{\infty}$ and $\varepsilon_{zz}^{\infty}$ are the principal components of the high-frequency dielectric tensor. The summation over μ covers all modes in the phonon bands of both layers. ε_{xx} has poles at each of the confined TO mode frequencies, and ε_{zz} has zeros at the confined LO frequencies. Expressions having the general form of Eq. (7) can be obtained from any model of phonon confinement that yields dielectric functions.

III. LONG-WAVELENGTH ELECTROSTATIC MODES

Electromagnetic wave propagation in a uniaxial medium represented by Eqs. (6) or (7) includes a polariton region at small wave vector ($q\sim\omega/c$). If one is merely interested in the phonon propagation, the polariton region can be excluded by using the unretarded limit in which $c\rightarrow\infty$; the modes are then simply electrostatic modes. The Maxwell equations $\mathbf{q}\cdot\mathbf{D}=0$ and $\mathbf{q}\times\mathbf{E}=0$ show that $\mathbf{D}$ is transverse to the wave vector $\mathbf{q}$, whereas $\mathbf{E}$ is directed along it. The fields $\mathbf{D}$ and $\mathbf{E}$ associated with unretarded phonons are therefore orthogonal, and satisfy the condition $\mathbf{D}\cdot\mathbf{E}=0$; although one or the other field must be zero for phonons propagating in special symmetry directions, in general both may be nonzero.

We take the wave vector $\mathbf{q}$ in the xz plane, with propagation angle θ such that $\tan\theta=q_x/q_z$. For p polarization (fields in the xz plane), $\mathbf{q}\cdot\mathbf{D}=0$ and $\mathbf{q}\times\mathbf{E}=0$ then give, respectively,

$$\tan\theta=-\varepsilon_{zz}\overline{E_z}/\varepsilon_{xx}\overline{E_x}\quad\text{and}\quad\tan\theta=\overline{E_x}/\overline{E_z}, \tag{8}$$

i.e.,

$$\tan^2\theta=-\varepsilon_{zz}(\omega)/\varepsilon_{xx}(\omega). \tag{9}$$

This equation relates propagation angle θ to frequency ω for p-polarized phonons, and can also be obtained by taking the unretarded limit ($c\to\infty$) into the p-polarization polariton equation[22]

$$q_x^2/\varepsilon_{zz}+q_z^2/\varepsilon_{xx}=\omega^2/c^2. \tag{10}$$

In s polarization ($\mathbf{D}$ fields in the y direction), the expression equivalent to Eq. (9) is just

$$\varepsilon_{xx}^{-1}=0, \tag{11}$$

showing that s-polarized phonons, less interestingly, have no angular dependence.

Equation (9) can be used to describe the angular behavior of long-wavelength p-polarized phonons, using any convenient model for the superlattice dielectric functions. Where the bulk slab model, represented by Eq. (6), is applicable, the equation describes phonons that are often referred to as interface modes. In this paper, we concentrate on confined phonon models that give dielectric functions of the form (7), using two models. The first is a simple continuum model that assumes that all vibrational amplitudes go to zero at the interfaces. The second is a microscopic linear-chain model that can be modified to include the effects of interface roughness. In each case, we calculate the phonon frequencies at general propagation angle θ using Eqs. (9) and (11), and calculate the corresponding phonon displacement patterns.

IV. CONTINUUM MODEL FOR THE DIELECTRIC FUNCTION

All microscopic fields $\mathcal{F}(\mathbf{r},t)$ in the superlattice structure are assumed to have the Bloch form (2). The electric displacement $\mathcal{D}$ satisfies the Maxwell equation $\nabla\cdot\mathcal{D}(\mathbf{r},t)=0$, so

$$i\mathbf{q}\mathbf{D}(z)+\frac{\partial D_z(z)}{\partial z}=0. \tag{12}$$

In the long-wavelength limit, $\mathbf{D}(z)$ can be expanded as a power series in qL:

$$\mathbf{D}(z)=\mathbf{D}^{(0)}(z)+\sum_\alpha \mathbf{D}_\alpha^{(1)}(z)q_\alpha L+\cdots . \tag{13}$$

Putting Eq. (13) into Eq. (12), the term of order $n=0$ in q is $dD_z^{(0)}/dz=0$, so to zero order in qL, $D_z(z)$ is constant and equal to the macroscopic average $\underline{D}_z$ over the superlattice period. Similarly, using $\nabla\times\mathcal{E}(\mathbf{r},t)=-\partial\mathcal{B}(\mathbf{r},t)/\partial t$, it can be shown that both $E_x(z)$ and $E_y(z)$ are effectively constant over the superlattice period to zero order in qL.

We now use a simple continuum model to obtain a form for the dielectric function in the long-wavelength limit, in which E_x, E_y, and D_z are uniform over the superlattice cell. First consider the in-plane motion. Since E_x is a constant, it is obviously appropriate to treat the in-plane component $u_x(z)$ of the atomic displacements as a response to this uniform field. We make the usual assumption that the atomic displacements are pinned at the boundary between the two media, so the displacement $u_x(z)$ in layer 1 can be written as a Fourier sum of mode displacements $u_m(z)=\sin(\pi mz/d_1)$ of the form of Eq. (1):

$$u_x(z)=\sum_m a_{1m}\sin(\pi mz/d_1)E_x \quad (0\leqslant z\leqslant d_1). \tag{14}$$

Assuming that each of the functions $u_m(z)$ is an eigenmode of the system, the coefficients a_{1m} will have the resonant response form

$$a_{1m}=\frac{A_{1m}}{\omega_{T1m}^2-\omega^2}. \tag{15}$$

Here ω_{T1m} is the eigenfrequency of the mode m, which, to a first approximation, will be the frequency $\omega_{\mathrm{TO1}}(\mathbf{k})$ of a bulk TO phonon in medium 1 with wave vector $\mathbf{k}=(0,0,m\pi/d_1)$:

$$\omega_{T1m}\approx\omega_{\mathrm{TO1}}(k_z=m\pi/d_1). \tag{16}$$

The displacements $u_x(z)$ of the optic-phonon modes cause a local ''phonon'' polarization $P_x(z)$, which we assume is proportional to $u_x(z)$. The local susceptibility $\chi_x(z)$, defined as

$$\chi_x(z)=\frac{\partial P_x(z)}{\varepsilon_0\partial E_x}, \tag{17}$$

has the form

$$\chi_x(z)=\sum_m \frac{r_{1m}}{\omega_{T1m}^2-\omega^2}\sin(\pi mz/d_1), \tag{18}$$

where r_{1m} are coefficients related to the coefficients in Eqs. (14) and (15).

In order to determine values for these coefficients r_{1m}, we examine the bulk slab limit for large d_1, when $\chi_x(z)$ becomes a constant and equal to the bulk phonon susceptibility χ_1 for layer 1. The relationship between the bulk electrostatic fields is

$$\mathbf{D}(z)=\varepsilon_1(\omega)\varepsilon_0\mathbf{E}(z)=\varepsilon_1^\infty\varepsilon_0\mathbf{E}(z)+\mathbf{P}(z),$$

where $\varepsilon_1(\omega)$ is given by Eq. (5), $\mathbf{P}(z)$ is the phonon polarization, and the high-frequency dielectric function ε_1^∞ incorporates the atomic polarization $\mathbf{P}_{\mathrm{at}}=(\varepsilon_1^\infty-1)\varepsilon_0\mathbf{E}$. The bulk-phonon polarization susceptibility is therefore

$$\chi_1=\varepsilon_1(\omega)-\varepsilon_1^\infty=\frac{\varepsilon_1^\infty\Delta_1^2}{\omega_{\mathrm{TO1}}^2-\omega^2} \quad\text{with}\quad \Delta_1^2=\omega_{\mathrm{LO1}}^2-\omega_{\mathrm{TO1}}^2, \tag{19}$$

In the bulk limit $d_1\to\infty$, $\chi_x(z)$ of Eq. (18) can be cast in the form of χ_1 in Eq. (19) by replacing the confined mode frequencies ω_{T1m} by the bulk value ω_{TO1} and using the identity

$$\frac{4}{\pi}\sum_{m\ \mathrm{odd}}^{\infty}\frac{1}{m}\sin(\pi mz/d_1)=1 \quad \text{in the range } 0<z<d_1 \tag{20}$$

to show that the coefficients r_{1m} have the values

$$r_{1m}=4\varepsilon_1^\infty\Delta_1^2\pi m \quad \text{for } m \text{ odd},$$

$$r_{1m}=0 \quad \text{for } m \text{ even}. \tag{21}$$

The modes of even m carry no electric dipole moment, and do not contribute to χ_x.

Assuming the values (21) for r_{1m} can be carried over to thin layers, the spatially-dependent susceptibility (18) becomes

$$\chi_x(z)=\sum_{m\ \text{odd}}\ \frac{4\varepsilon_1^{\infty}\Delta_1^2}{m\pi(\omega_{T1m}^2-\omega^2)}\sin(\pi mz/d_1)\quad(0\leqslant z\leqslant d_1),\tag{22}$$

with the average susceptibility for layer 1 given by

$$\langle\chi_x\rangle_1=\frac{1}{d_1}\int_0^{d_1}\chi_x(z)dz=\sum_{m\ \text{odd}}\ \frac{8\varepsilon_1^{\infty}\Delta_1^2}{\pi^2m^2(\omega_{T1m}^2-\omega^2)}.\tag{23}$$

All of the above procedure may be repeated for layer 2. Overall, one can then relate the microscopic polarization $P_x(z)$ and the electric displacement $D_x(z)$ to the uniform field E_x through spatially-dependent susceptibilities $\chi_x(z)$ and $\varepsilon_{xx}(z)$:

$$P_x(z)=\varepsilon_0\chi_x(z)E_x\quad D_x(z)=\varepsilon_0\varepsilon_{xx}(z)E_x,$$

where $\varepsilon_{xx}(z)=\underline{\varepsilon_j^{\infty}}+\chi_x(z)$ in layer i. The macroscopic fields are related by $D_x=\varepsilon_0\varepsilon_{xx}E_x$, where ε_{xx} is the spatial average $\langle\varepsilon_{xx}(z)\rangle$:

$$\varepsilon_{xx}=\frac{\partial\overline{D_x}}{\varepsilon_0\partial E_x}=[d_1(\varepsilon_1^{\infty}+\langle\chi_x\rangle_1)+d_2(\varepsilon_2^{\infty}+\langle\chi_x\rangle_2)]/(d_1+d_2).\tag{24}$$

This is of the same form as Eq. (7), with

$$\varepsilon_{xx}^{\infty}=(d_1\varepsilon_1^{\infty}+d_2\varepsilon_2^{\infty})/(d_1+d_2).\tag{25}$$

A similar approach to the above may be used in calculating ε_{zz}. In this case D_z is the appropriate driving field, because this is uniform throughout the superlattice. The appropriate local susceptibility $\xi_z(z)$ represents the response of the z displacements to the field D_z, and is defined as

$$\xi_z(z)=\partial P_z(z)/\partial D_z,\tag{26}$$

and the expression analogous to Eq. (22) is

$$\xi_z(z)=\sum_{m\ \text{odd}}\ \frac{4\Delta_1^2}{\pi m(\omega_{L1m}^2-\omega^2)}\sin(\pi mz/d_1),\tag{27}$$

where ω_{L1m} is the frequency of the mth confined LO mode in layer 1. The average susceptibility in layer 1 is then

$$\langle\xi_z\rangle_1=\sum_{m\ \text{odd}}\ \frac{8\Delta_1^2}{\pi^2m^2(\omega_{L1m}^2-\omega^2)},\tag{28}$$

and similarly for layer 2. One can thus obtain the position-dependent susceptibility

$$\varepsilon_{zz}^{-1}(z)=\frac{\varepsilon_0\partial E_z(z)}{\partial D_z},$$

and the average dielectric tensor component

$$\varepsilon_{zz}^{-1}=\frac{\varepsilon_0\partial\overline{E_z}}{\partial D_z}=[(1-\langle\xi_z\rangle_1)d_1/\varepsilon_1^{\infty}+(1-\langle\xi_z\rangle_2)d_2/\varepsilon_2^{\infty}]/(d_1+d_2),\tag{29}$$

of the same form as Eq. (7), with $\varepsilon_{zz}^{\infty}$ given by

$$(\varepsilon_{zz}^{\infty})^{-1}=(d_1/\varepsilon_1^{\infty}+d_2/\varepsilon_2^{\infty})/(d_1+d_2).\tag{30}$$

Expressions (24) and (30) for ε_{xx} and ε_{zz} describe the long-wavelength dielectric behavior of the superlattice, both in the polariton region ($q\sim\omega/c$) and in the unretarded phonon limit ($\omega/c\ll q\ll L^{-1}$), with Eqs. (9) or (10) providing a relation between frequency ω and angle of propagation θ. Calculations of mode frequencies ω as functions of angle θ and associated displacement $\mathbf{u}(z)$ are described in Sec. VI. The displacements $\mathbf{u}(z)$ are proportional to the polarization $\mathbf{P}(z)$, whose components are $P_x(z)=\chi_x(z)\ \varepsilon_0E_x$ and $P_z(z)=\xi_z(z)\ D_z$, and the relative amplitudes of the uniform fields D_z and E_x can be obtained from $\mathbf{q}\cdot\mathbf{D}=0$:

$$D_z/E_x=-\varepsilon_{xx}\varepsilon_0\ \tan\ \theta.\tag{31}$$

Finally, it is worth commenting on the electrostatic potential $\mathcal{V}(\mathbf{r},t)$ associated with the excitations, in the electrostatic (unretarded) and long-wavelength ($\mathbf{q}\rightarrow 0$) limits. The potential is related to the electric field by $\boldsymbol{\mathcal{E}}(\mathbf{r},t)=-\nabla\mathcal{V}(\mathbf{r},t)$, and $\mathcal{V}(\mathbf{r},t)$ takes the Bloch form

$$\mathcal{V}(\mathbf{r},t)=V(z)e^{i(\mathbf{q}\cdot\mathbf{r}-\omega t)}\quad\text{with}\ \ V(z+L)=V(z)$$

where $V(z)$ is given by

$$V(z)=iE_x/q_x-\varepsilon_0^{-1}D_z\int_0^z dz'[\varepsilon_{zz}^{-1}(z')-\varepsilon_{zz}^{-1}].$$

V. MICROSCOPIC MODEL OF DIELECTRIC FUNCTION

In this section, we briefly review the procedure for calculation of the susceptibilities in the form of Eq. (7), using the random element isodisplacement (REI) model. A full description of this model is given by Samson *et al.*[8] and also in the review by Dumelow *et al.*,[24] so we merely outline the important features here; the model has also been investigated by Bechstedt, Gerecke, and Grille.[25] The REI model evaluates the propagation of phonons along the z axis of the superlattice structure, represented as a diatomic linear A-B chain. The A sites contain As atoms, while the B sites are either Ga or Al, or indeed a proportion x of Ga and $(1-x)$ of Al, since the response is effectively that of the plane of atoms normal to the z axis. By choosing the force constants of the model to describe as accurately as possible the (100) dispersion curves for bulk GaAs and AlAs and the alloy mode frequencies, the model gives an accurate calculation of the phonon frequencies in GaAs/AlAs superlattices. Unlike the continuum model, the microscopic model needs no assumptions about how the displacements behave at the interface between the two constituent materials.

Interface roughness has a very important effect on the confined mode frequencies in short-period superlattices. The model of Samson *et al.*[8] enables the effects of interface roughness (or interface alloying) to be investigated by prescribing values of x for each B site that are not merely either 0 or 1. A simple approach is to characterize the roughness by a parameter W, such that the concentration $x_{\text{Ga},j}$ of Ga atoms at site z_j monolayers away from an interface has the error function form

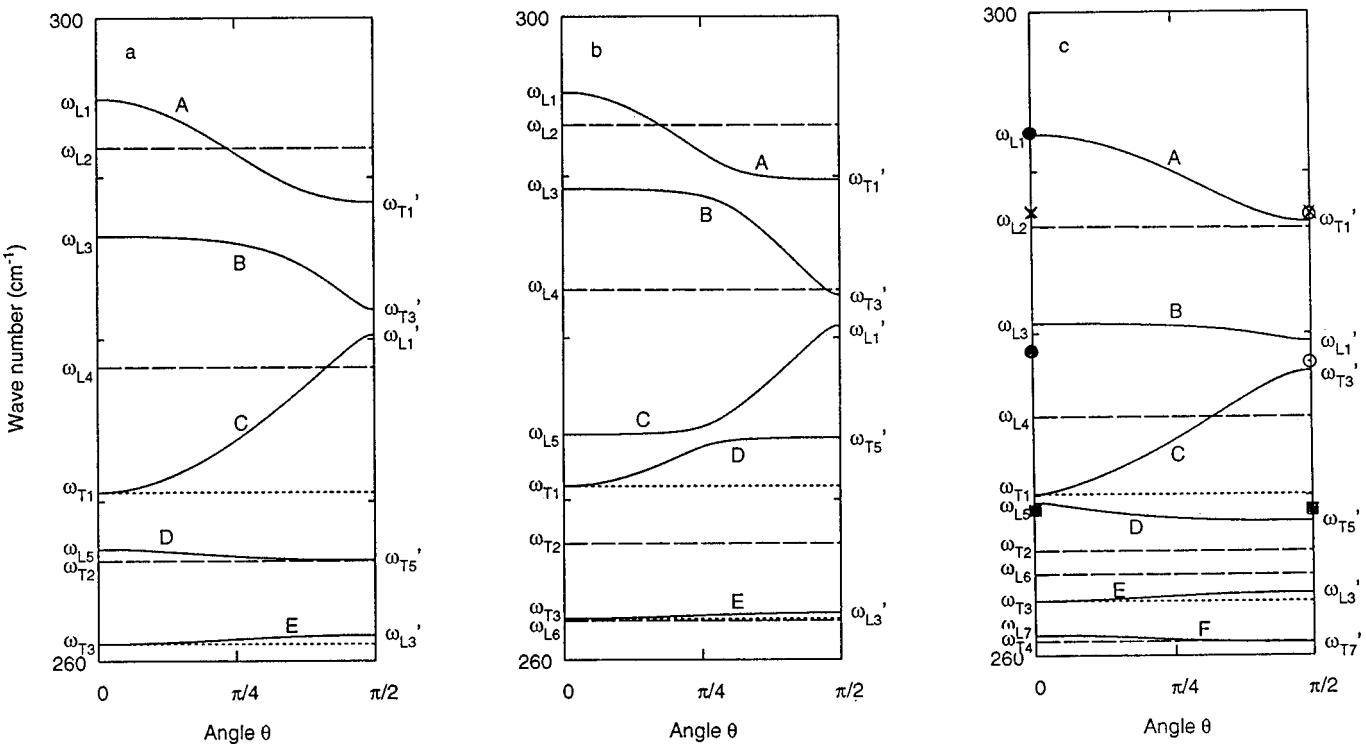

FIG. 1. Angular variation of GaAs-like mode frequencies at $q\rightarrow 0$ in a $(GaAs)_7(AlAs)_7$ superlattice, calculated according to Eq. (8): (a) continuum model; (b) microscopic model with interface broadening $W=0$; (c) microscopic model with $W=2.0$. The measured frequencies of Scamarcio *et al.* (Ref. 33) are shown as ●, LO_m modes (m odd) at $\theta=0$; ×, LO_m modes (m even); ■, TO_m modes (m odd); ○, TO modes.

$$x_{\mathrm{Ga},j}\approx\frac{1}{2}\left[1+\mathrm{erf}\left\{\frac{z_j}{W}\right\}\right]. \tag{32}$$

Samson *et al.* find the dynamical matrix $\underline{\underline{\mathbf{Y}}}$ that couples the normalized displacements e_{sj} $(=u_{sj}\sqrt{M_s}x_{sj}$, where M_s is the atomic mass) for atom type s in the cell j using a one-dimensional linear-chain model; they obtain a site response to applied fields $f_{s'j'}$ in the form

$$e_{sj}=\sum_{s'j'} f_{s'j'}\chi_{sj,s'j'} \quad \text{with} \quad \chi_{sj,s'j'}=\sum_{\mu}\frac{v_{sj,\mu}v^{*}_{s'j',\mu}}{\omega_\mu^2-\omega^2}, \tag{33}$$

where $v_{sj,\mu}$ is the matrix that diagonalizes $\underline{\underline{\mathbf{Y}}}$ with eigenvalues ω_μ^2. The functions $v_{sj,\mu}$ have a very similar form to the functions $\sin(\pi m z_j/d_1)$ in Eq. (1), with $m\equiv\mu$ and $z_j\equiv j_a$ (with a the lattice constant), and are identical in the limit of large d_1 and d_2. Eq. (33) is of the same form as Eq. (18), and to complete the analysis in order to obtain dielectric functions ε_{zz} and ε_{xx} analogous to Eqs. (24) and (29), values for the effective charges Q_{sj} involved in coupling the site displacements e_{sj} to the appropriate fields are estimated by recourse to the bulk dielectric functions (19).

VI. RAMAN SCATTERING INTENSITIES

Hayes and Loudon[26] give an expression for the Raman-scattering differential cross section in polar materials, which can be reduced to the following form:

$$\frac{d^2\sigma}{d\Omega\ d\omega_s}\sim I(\mathbf{e}_I\mathbf{e}_S,\mathbf{q})[n(\omega)+1],$$

where

$$I(\mathbf{e}_I,\mathbf{e}_S,\mathbf{q})=\sum_{iji'j'} e_S^i e_I^j e_S^{i'} e_I^{j'}\,\mathrm{Im}\Bigg\{-\Bigg[\sum_{hh'}(a^{ijh}\chi_h+b^{ijh})\times(a^{a'j'h'}\chi_{h'}+b^{i'j'h'})q_h q_{h'}\Bigg]\Big/ f+\sum_h a^{ijh}a^{i'j'h}\chi_h\Bigg\}. \tag{34}$$

Here, the (unit) polarization vectors of the incident and scattered light are $\mathbf{e}_I$ and $\mathbf{e}_S$, with components denoted by indices i and j $(=x,y,z)$. χ_h denotes the susceptibility

$$\chi_h=\frac{\partial P_h}{\varepsilon_0\partial E_h} \quad (h=x,y,z), \tag{35}$$

assumed to be diagonal in the crystallographic axes x,y,z. $\chi_h(\omega)$ has poles at the TO frequencies $\omega_{h\mu}$. q_h is the component of the phonon propagation vector along the h axis, and f is the polar mode dielectric function,

$$f=(q_x^2+q_y^2)\varepsilon_{xx}+q_z^2\varepsilon_{zz}, \tag{36}$$

in which the dielectric functions ε_{hh} and the susceptibilities χ_h are related by

$$\varepsilon_{hh}=\varepsilon_{hh}^{\infty}+\chi_h, \tag{37}$$

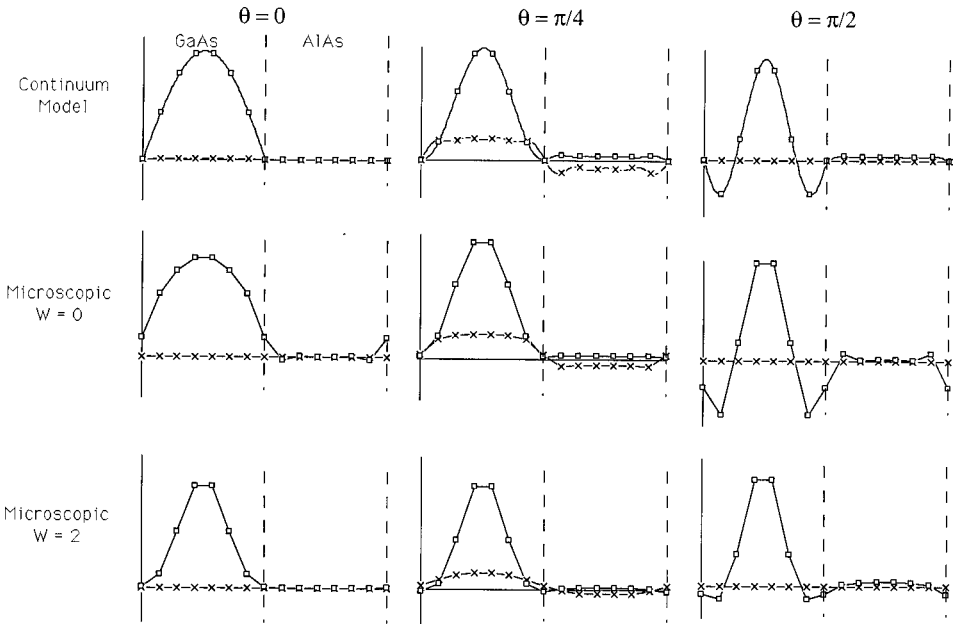

FIG. 2. Displacement patterns for modes at $\theta=0$, $\pi/4$, and $\pi/2$ for mode A of Fig. 1 (the LO_1 mode at $\theta=0$): □, z displacements; ×, x displacements.

with $\varepsilon_{xx}=\varepsilon_{yy}$ because of the tetragonal symmetry of the superlattice.

a^{ijh} is a coupling coefficient, which in principle is different for each of the modes μ contributing to χ_h and in writing down Eq. (34) we have in effect assumed that the Raman coupling coefficient of each mode is proportional to its infrared strength. Furthermore, we shall approximate a^{ijh} by assuming that it has the symmetry properties of the bulk zinc-blende structure, namely,

$$a^{ijh}=0 \quad \text{unless} \quad i\neq j\neq h\neq i, \tag{38}$$

and we also assume that the nonzero values of a^{ijh} can all be put equal to a single parameter a when considering phonons in the GaAs reststrahl region. The part of the Raman-scattering cross section involving the coefficients a^{ijh} arises from coupling of light to phonon displacements via the deformation potential. The coefficient b^{ijh} is the electro-optic coefficient that describes coupling to the macroscopic fields associated with the phonon, usually described as the Fröhlich interaction. We make the same symmetry assumptions (38) for the b^{ijh} parameters as for a^{ijh}; for bulk GaAs, Hayes and Loudon quote

$$b/a=-0.17\,\frac{\varepsilon^{\infty}\Delta^2}{\omega_{\mathrm{TO}}^2} \quad \text{with} \quad \Delta^2=\omega_{\mathrm{LO}}^2-\omega_{\mathrm{TO}}^2. \tag{39}$$

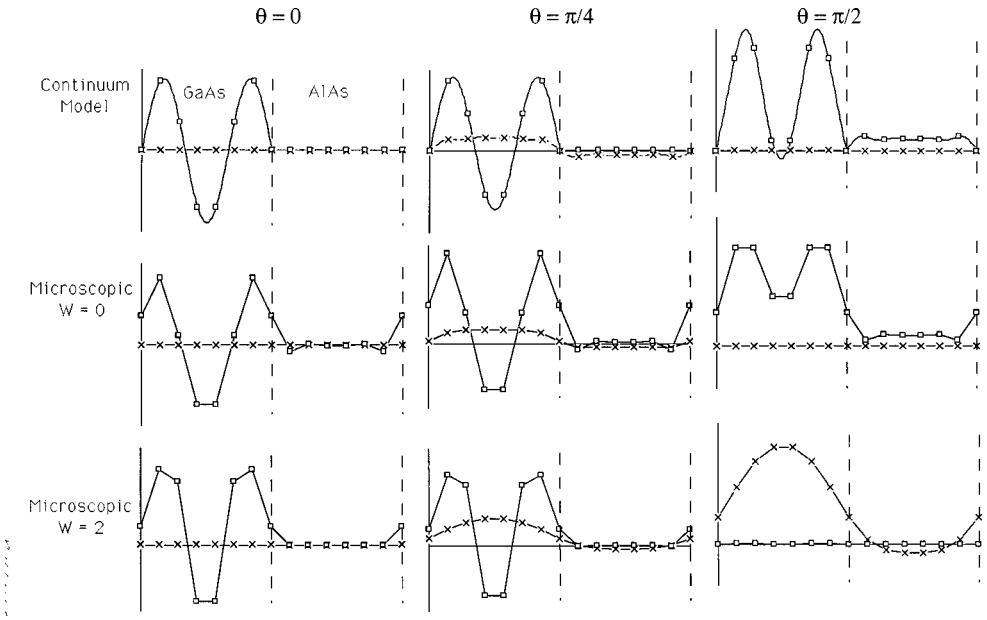

FIG. 3. Displacement patterns for modes at $\theta=0$, $\pi/4$, and $\pi/2$ for mode B of Fig. 1 (the LO_3 mode at $\theta=0$): □, z displacements; ×, x displacements.

TABLE I. Definition of axes used in Raman scattering calculations.

Axes	Directions of components		
(x,y,z)	$x \equiv (100)$	$y \equiv (010)$	$z \equiv (001)$
(x',y',z)	$x' \equiv \sqrt{\frac{1}{2}}(110)$	$y' \equiv \sqrt{\frac{1}{2}}(\overline{1}10)$	$z \equiv (001)$
(X,y,Z)	$X \equiv \sqrt{\frac{1}{2}}(101)$	$y \equiv (010)$	$Z \equiv \sqrt{\frac{1}{2}}(\overline{1}01)$
(X',y',Z')	$X' \equiv \frac{1}{2}(11\sqrt{2})$	$y' \equiv \sqrt{\frac{1}{2}}(\overline{1}10)$	$Z' \equiv \frac{1}{2}(\overline{1}\ 1\sqrt{2})$

Note that the coupling considered here is the same as that which gives the Raman scattering in the bulk materials, and will consequently involve only the odd index m modes. Strictly speaking, the superlattice symmetry is lower than the bulk (D_{2d} rather than T_d), so neither the restriction (38) nor the assumption of single parameters a and b is rigorously valid. This becomes apparent under resonant excitation conditions, when scattering from even index modes is observable via a version of the Fröhlich interaction which acts through the intrasubband effect of the electric potential associated with the phonons.[27] We ignore this possibility in the present analysis and restrict our attention to nonresonant excitation conditions, although the analysis may also be reasonably valid for the odd index scattering under resonant conditions with the proviso that the parameters a and b will be differently affected by the resonance.

The expression (34) produces resonances of two types: (a) when the denominator f is zero, the resonances correspond to the p-polarized modes of Eq. (9) (sometimes referred to as polar modes); (b) when there are poles in the susceptibilities χ_h, TO resonances appear in both terms in the curly brackets in Eq. (34), though these resonances can be canceled in certain geometries.

We will consider various cases, in which the phonon propagation is described by the usual polar angles θ and ϕ. Then $\mathbf{q}$ is the vector $q(\sin\theta\cos\phi, \sin\theta\sin\phi, \cos\theta)$, and

$$f = q^2(\sin^2\theta\ \varepsilon_{xx} + \cos^2\theta\ \varepsilon_{zz}). \tag{40}$$

Calculated spectra using Eq. (34) are shown in the next section.

VII. CALCULATIONS OF MODE FREQUENCIES AND DISPLACEMENTS

In this section we calculate the angular variation of the mode frequencies and displacements using the two dielectric function models outlined above. Where appropriate, our modeled results are compared with published experimental micro-Raman measurements.

Figure 1 shows the dependence of the GaAs-like mode frequencies in a $(GaAs)_7(AlAs)_7$ superlattice on propagation angle θ. The mode frequencies satisfy Eqs. (9) and (10). Three different models have been used for the dielectric function: the continuum model outlined in Sec. III has been used to model Fig. 1(a), and the linear-chain model described in Sec. IV has been used in Figs. 1(b) and 1(c), without and with interface roughness ($W=0$ and $W=2.0$, respectively). The continuum model derives its confined mode frequencies $\omega_{\mathrm{LO}m}$ and $\omega_{\mathrm{TO}m}$ from the same bulk phonon dispersion as is used in the linear-chain model.

As $\theta \to 0$, Eq. (9) has solutions when either $\varepsilon_{zz}(\omega) \to 0$ or $\varepsilon_{xx}(\omega)^{-1} \to 0$, and the modes are classified correspondingly as LO_m or TO_m with displacements parallel or normal to the axis of propagation, respectively. The modes with m even (shown by dashed lines in Fig. 1) carry no dipole moment and so they do not contribute to the dielectric functions and show no angular variation. The s-polarized solutions $\varepsilon_{xx}(\omega)^{-1}=0$ of Eq. (10) persist regardless of angle, and are shown in Fig. 1 as dotted lines. The remaining modes are the dipole-active p-polarized modes, and show angular dependence required by Eq. (9). At $\theta=\pi/2$ (propagation in the x-y plane) these modes can be classified as TO'_m or LO'_m according to whether they are solutions of $\varepsilon_{zz}(\omega)^{-1}=0$ or $\varepsilon_{xx}(\omega)=0$, and have displacements along z or along the wave vector direction, respectively. We have used odd indices m to label dipole active TO'_m and LO'_m modes at $\theta=\pi/2$, but unlike the situation at $\theta=0$ the index m does not necessarily represent the number of confined phonon half-wavelengths, as will be apparent when the mode patterns are examined.

The continuum model results are similar to those obtained from other continuum models.[16,18,28] The long-wavelength limit of the model of Chamberlain, Cardona, and Ridley,[28] for instance, is equivalent to the model presented here provided that the phonon dispersion is parabolic, that the modes

TABLE II. Relative intensity factors I for various Raman-scattering geometries, with propagation angle θ and mode classification type. Definitions of axes are given in Table I.

Scattering geometry	Relative intensity factor I	Angle θ	Mode type
$z(xy)\overline{z}$ or $z(y'y')\overline{z}$	$\mathrm{Im}\{-(\chi_z+b)^2/\varepsilon_{zz}+\chi_z\}$	0	LO_m
$Z(Xy)\overline{Z}$	$\mathrm{Im}\{-\frac{1}{2}(\chi_x-\chi_z)^2/(\varepsilon_{xx}+\varepsilon_{zz})+\frac{1}{2}(\chi_x+\chi_z)\}$	$\pi/4$	mixed
$Z'(X'X')\overline{Z'}$	$\mathrm{Im}\{-\frac{1}{4}(2\chi_x-\chi_z+b)^2/(\varepsilon_{xx}+\varepsilon_{zz})+\frac{1}{4}\chi_x+\chi_z\}$	$\pi/4$	mixed
$Z'(y'y')\overline{Z'}$	$\mathrm{Im}\{-(\chi_z+b)^2/(\varepsilon_{xx}+\varepsilon_{zz})+\chi_z\}$	$\pi/4$	mixed
$Z(XX)\overline{Z}$	$\mathrm{Im}\{\chi_x\}$	$\pi/4$	TO_m
$x'(y'z)\overline{x'}$	$\mathrm{Im}\{\chi_x\}$	$\pi/2$	TO_m
$x'(y'y')\overline{x'}$	$\mathrm{Im}\{\chi_z\}$	$\pi/2$	TO'_m
$x(yz)\overline{x}$	$\mathrm{Im}\{-(\chi_x+b)^2/\varepsilon_{xx}+\chi_x\}$	$\pi/2$	LO'_m

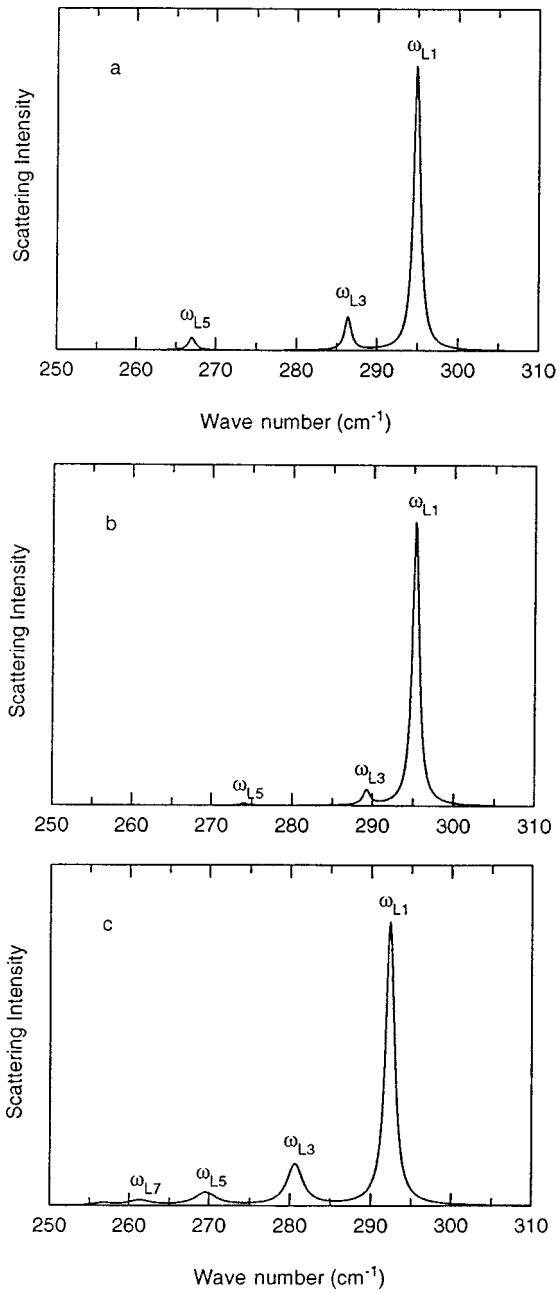

FIG. 4. Calculated nonresonant Raman backscattering $z(xy)\bar{z}$ spectra for a $(GaAs)_7(AlAs)_7$ superlattice, obtained using Eq. (34) for the three models of Fig. 1: (a) continuum model; (b) microscopic model with $W=0$; (c) microscopic model with $W=2.0$.

in Eq. (22) and (27) are summed to infinity, and that the phonons in the AlAs layer make no contribution. The present model has the advantage over other continuum models in that none of the above assumptions are necessary. Moreover, it is simpler to use, requiring only numerical substitution into simple algebraic expressions, although, in the form presented here, it is restricted to the long-wavelength limit.

The three plots in Fig. 1 show some qualitative differences. For instance, the curve corresponding to LO_3 at $\theta=0$ extends to ω'_{T3} in Figs. 1(a) and 1(b), but extends to ω'_{L1} in Fig. 1(c). This type of behavior depends on the relative frequencies of the poles and zero in ε_{xx} in comparison to the poles and zeros in ε_{zz}. It is particularly striking that interface roughness appears to affect the results more than whether the model used is microscopic or continuum in nature. In fact, the results of the continuum model shown in Fig. 1(a) are in effect intermediate between the microscopic model results of Figs. 1(b) and 1(c), particularly in respect of the higher-frequency modes.

Figures 2 and 3 show the displacement patterns associated with the two highest-frequency modes *A* and *B* of Fig. 1 (the $\theta=0$ LO_1 and LO_3 modes). The mode patterns are calculated using each of the three models used in Fig. 1 and are shown at $\theta=0$, $\pi/4$, and $\pi/2$. Note that in the continuum model the displacement inevitably falls to zero at the interfaces, but in the microscopic model the vibrations more plausibly extend slightly into the AlAs layer. Consequently, the confinement is less than in the continuum model with the result that the microscopic model gives slightly higher mode frequencies than the continuum model. This effect has long been recognized; some authors using the continuum model extend the effective width of the active layer by one monolayer unit in order to model the mode frequencies quantitatively correctly.[28] Interface roughness can markedly affect the mode frequencies and displacements. As can be seen in the displacement patterns in Figs. 2 and 3, the modes are more confined when the interfaces are rough. This is because the rough interfaces, which can be considered as thin alloy layers, are effectively acting as barriers to the phonon vibrations. The inclusion of interface roughness therefore tends to lower confined mode frequencies, as observed in Fig. 1(c) and as pointed out by many authors.[7,8,29] At lower frequencies, the interface alloy layers no longer act as barriers, and vibrations extend further into the AlAs layers, decreasing confinement. These modes appear at a higher frequency than the equivalent modes for a superlattice having sharp interfaces.

Looking in detail at the mode patterns shown in Figs. 2 and 3, it is clear that, while the displacement patterns at $\theta=0$ have the basic sinusoidal form $u_m(z)\sim\sin(m\pi z/d)$, they become much less simple away from $\theta=0$. Here, the coupling between the mode displacements and the macroscopic electrostatic fields causes the odd-index *p*-polarized modes to contain significant contributions from a number of eigenmodes u_m, so the mode index *m* on these modes does not necessarily directly denote the number of phonon half-wavelengths confined in the GaAs layer: for example, the $\theta=\pi/2$ continuum mode $\omega_{T1'}$ is clearly composed primarily of $m=1$ and $m=3$ modes. The *x* displacements for the modes shown in Figs. 2 and 3 appear to have a simpler form with a single antimode, but at lower frequencies within the bulk TO band the *x* displacements show more prominent oscillatory confinement patterns. The AlAs optic-phonon bands are at higher frequencies than the GaAs optic bands, so all models only show small displacements in the AlAs layer at the GaAs-like frequencies.

VIII. CALCULATIONS OF RAMAN SPECTRA

We now consider the Raman spectra corresponding to the expression (34) in Sec. VI. Over the past few years there has been a number of publications of Raman spectra from GaAs/AlAs superlattices with nonzero propagation angles θ, and without making an exhaustive comparison with experiment

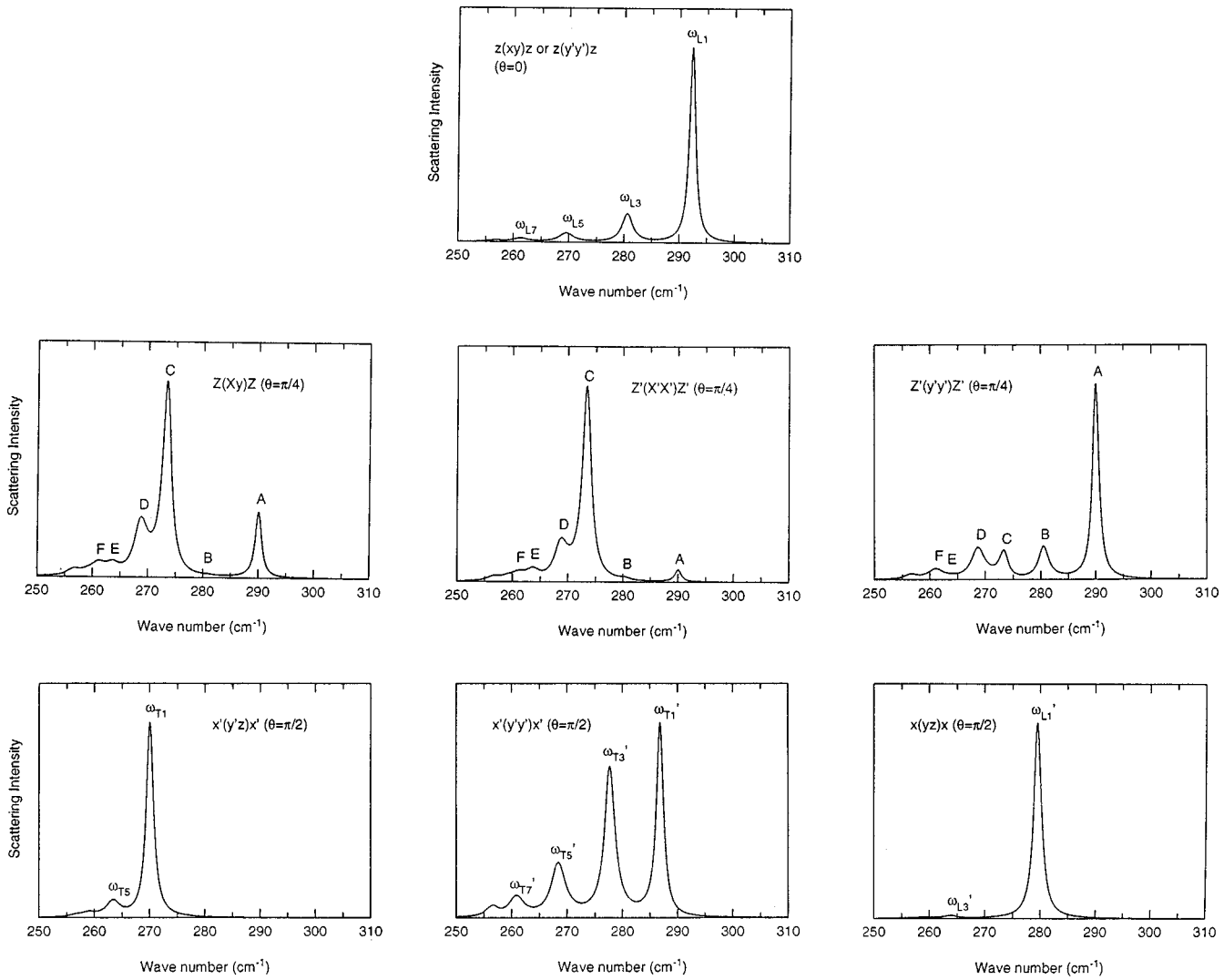

FIG. 5. Nonresonant Raman-scattering intensities calculated using Eq. (34) for a $(GaAs)_7(AlAs)_7$ superlattice, with the scattering geometries: $z(xy)\bar{z}$ or $z(y'y')\bar{z}$ $(\theta=0)$; $Z(Xy)Z$ $(\theta=\pi/4)$; $Z'(X'X')Z'$ $(\theta=\pi/4)$; $Z'(y'y')Z'$ $(\theta=\pi/4)$; $Z(XX)Z$ $(\theta=\pi/4)$ [equivalent to $x'(y'z')\bar{x}'$ $(\theta=\pi/2)$]; $x'(y'y')\bar{x}'$ $(\theta=\pi/2)$; $x(yz)\bar{x}$ $(\theta=\pi/2)$. See text for definitions of axes.

we want to point out that our approach gives a simple description of the intensities as well as the frequencies of the modes observed in such experiments. As far as we are aware, no attempt has hitherto been made to model the intensities of the spectra, which show a remarkably rich variation with propagation direction and scattering geometry. Scattering geometries that are of particular interest involve the sets of axes listed in Table I. The following expressions are obtained for the relative intensity factors $I(\mathbf{e}_I,\mathbf{e}_S,\mathbf{q})$ for nonresonant Raman scattering, using the conventional notation $\hat{\mathbf{q}}_I(\mathbf{e}_I,\mathbf{e}_S)\hat{\mathbf{q}}_S$, in which $\hat{\mathbf{q}}_I$ and $\hat{\mathbf{q}}_S$ are the propagation directions of the incident and scattered photons, with polarizations $\mathbf{e}_I$ and $\mathbf{e}_S$, respectively. Table II gives the results calculated from Eq. (34) (with $a=1$) for some backscattering geometries of experimental interest.

As an illustration, in Fig. 4 we show the calculated backscattering $z(xy)\bar{z}$ nonresonant Raman spectra, obtained using Eq. (34), for the three models of Fig. 1. Mode damping was obtained for the microscopic model as described by Samson *et al.*,[8] using the same parameters. In this orientation, odd-index LO_m modes should be observed at the frequencies corresponding to $\theta=0$ in Fig. 1. In practice, experimental investigations often include resonant Raman scattering, where the scattering also involves the Fröhlich electric potential interaction, which gives an angularly invariant contribution from the even-index modes observable in certain scattering geometries; we do not cover this contribution here.

In Fig. 5 we compare calculated backscattering spectra for a number of different geometries corresponding to $\theta=0$, $\pi/4$, and $\pi/2$. In all cases the dielectric function is the same as was used to model Fig. 1(c), i.e., that obtained from the microscopic model with interface roughness. It can be seen how different modes arise from the selection rules implicit in Eq. (34). In addition, the spectra show that the relative intensities also depend on the scattering geometry. The mode frequencies, in contrast, depend only on the angle θ.

We now compare our results with those obtained experimentally. As yet, there have been few $\theta\neq 0$ measurements on superlattices with sufficiently thin layers to show appreciable confinement. Hessmer *et al.*[30] report backscattering micro-Raman results over a series of angles for superlattices

having GaAs wells of width about 10 nm. The layers in these samples are sufficiently thick that a microscopic model is not required, and the results can be interpreted using the bulk slab model represented by Eqs. (1) and (2). Similarly Fainstein *et al.*[31] have used 90° scattering to investigate a superlattice with a GaAs width of 5 nm. Although they interpret their results in terms of confined modes using a continuum model, represented by Eqs. (1) and (2), their results are essentially the same as those obtained using the bulk slab model. Haines and Scamarcio[32] and Scamarcio *et al.*[33] have made backscattering measurements on short-period GaAs/AlAs superlattices for both $\theta=0$ and $\theta=\pi/2$ using a number of different scattering geometries. Zunke *et al.*[34] have also made backscattering measurements, in this case corresponding to a series of intermediate values of θ, but with the polarization of incoming and outgoing radiation restricted to the y' direction, for which unequivocal mode assignments are not possible. Since the assignments of Zunke *et al.* appear to differ significantly from those by other authors on similar samples,[32,33] we restrict ourselves to modeling the spectra of Scamarcio *et al.*[33] The unit cell of one of the samples, $(GaAs)_{2.5}(AlAs)_{1.1}$ reported in their paper is so far off stoichiometry as to make microscopic modeling unreasonable, but we have modeled all the other results.

Scamarcio *et al.*[33] show experimental Raman-scattering spectra for a $(GaAs)_7(AlAs)_7$ superlattice with the scattering geometries $z(xy)\bar{z}$, $z(yy)\bar{z}$, $x(yy)\bar{x}$, $x(yz)\bar{x}$, $z(y'y')\bar{z}$, $x'(y'y')\bar{x'}$, and $x'(zy')\bar{x'}$. The geometries $z(yy)\bar{z}$ and $x(yy)\bar{x}$ produce no features in nonresonant scattering, but show an LO_2 feature due to the Fröhlich interaction. Apart from the $x(yz)\bar{x}$ spectrum, there is close agreement between the experimental spectra and those shown in Fig. 4, modeled with an interface width of $W=2.0$, although the $z(y'y')\bar{z}$ and $x'(y'y')\bar{x'}$ spectra yield additional LO_2 contributions. The experimental results for the $x(yz)\bar{x}$ geometry are somewhat unclear. This may be because the quality of the polished (100) surface was not as good as for the cleaved (110) surface, resulting in a relaxation of the selection rules.

The experimental frequencies obtained from the $(GaAs)_7(AlAs)_7$ spectra of Scamarcio *et al.* are included on Fig. 1(c). It can be seen that neither the continuum model nor the linear-chain model with no roughness would successfully model the experimental data. When an interface width of 2.0 ML is included in the linear-chain model, however, the agreement is excellent. It thus appears that interface roughness is an important parameter in determining the phonon behavior. Note, however, that the repeat unit, as measured by x-ray scattering, was $(GaAs)_{7.5}(AlAs)_{6.8}$, so the value $W=2.0$ for our interface roughness parameter may to some extent incorporate the difference between this and the assumed superlattice $(GaAs)_7(AlAs)_7$.

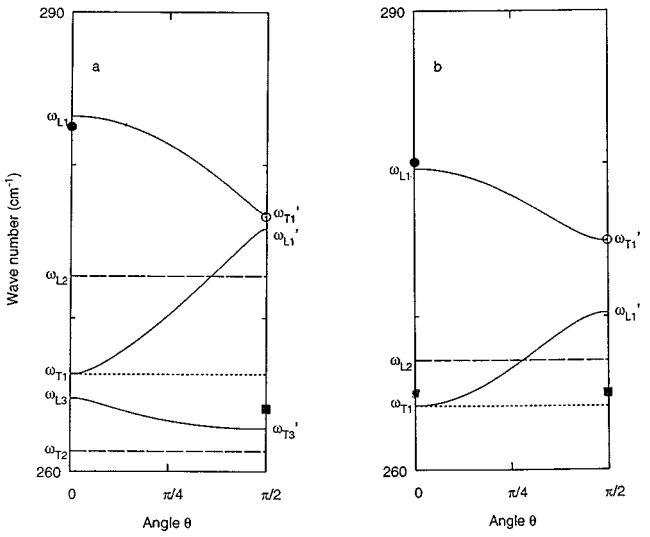

FIG. 6. Angular variation of GaAs-like mode frequencies at $q\rightarrow 0$: (a) $(GaAs)_3(AlAs)_3$ superlattice ($W=1.4$); (b) $(GaAs)_2(AlAs)_4$ superlattice ($W=1.0$). The measured frequencies of Scamarcio *et al.* (Ref. 33) are shown as in Fig. 1.

The experimental frequencies for the other samples studied by Scamarcio *et al.* are compared with theory in Fig. 6. We have only shown theoretical curves for the microscopic model with interface roughness, because in all cases considerably better fits are obtained with roughness included. In each case a best-fit value for interface roughness is used. However, x-ray diffraction has shown that in none of these samples is each layer an integral number of lattice units wide. As with the $(GaAs)_7(AlAs)_7$ superlattice, therefore, the modeled interface width may not accurately reflect the true value of the roughness.

The above results show that micro-Raman results can be modeled qualitatively using a continuum model in a simple manner. More quantitative results require the use of a model that incorporates interface roughness, and excellent agreement with experiment can be obtained in this case. We have also shown how the use of a number of different scattering geometries can lead to unequivocal mode assignments.

ACKNOWLEDGMENTS

The authors wish to acknowledge useful discussions with N. C. Constantinou and M. P. Chamberlain.

*Present address: Departamento de Fisica, Universidade Federal do Rio Grande do Norte, Caixa Postal 1641, 59072-970 Natal RN, Brasil.

[1] K. Kunc and R. M. Martin, Phys. Rev. Lett. **48**, 406 (1982).
[2] B. Jusserand, F. Alexandre, D. Paquet, and G. Le Roux, Appl. Phys. Lett. **47**, 301 (1985).
[3] E. Molinari, A. Fasolino, and K. Kunc, Superlattices Microstruct. **2**, 379 (1986).
[4] B. Jusserand, Phys. Rev. B **42**, 7256 (1990).
[5] A. Fasolino, E. Molinari, and K. Kunc, Phys. Rev. B **41**, 8302 (1990); A. Fasolino and E. Molinari, Surf. Sci. **228**, 112 (1990).
[6] S. Baroni, P. Giannozzi, and E. Molinari, Phys. Rev. B **41**, 3870 (1990).
[7] E. Molinari, S. Baroni, P. Giannozzi, and S. de Girancoli, Phys. Rev. B **45**, 4280 (1992).
[8] B. Samson, T. Dumelow, A. A. Hamilton, T. J. Parker, S. R. P. Smith, D. R. Tilley, C. T. Foxon, D. Hilton, and K. J. Moore, Phys. Rev. B **46**, 2375 (1992).
[9] H. Chu and Y.-C. Chang, Phys. Rev. B **38**, 12 369 (1988).

[10] H. Chu, S.-F. Ren, and Y.-C. Chang, Phys. Rev. B **37**, 10 746 (1988).
[11] S.-F. Ren, H. Chu, and Y.-C. Chang, Phys. Rev. B **37**, 8899 (1988).
[12] Y. Chang, S. Ren, and H. Chu, Superlattices Microstruct. **9**, 383 (1991).
[13] F. Bechstedt and H. Gerecke, Phys. Status Solidi B **154**, 565 (1989).
[14] R. Fuchs and K. L. Kliewer, Phys. Rev. **140**, A2076 (1965).
[15] M. Babiker, J. Phys. C **19**, 683 (1986).
[16] K. Huang and B. Zhu, Phys. Rev. B **38**, 13 377 (1988).
[17] B. K. Ridley, Phys. Rev. B **44**, 9002 (1991).
[18] B. K. Ridley, Phys. Rev. B **47**, 4592 (1993).
[19] N. C. Constantinou, O. Al-Dossary, and B. K. Ridley, Solid State Commun. **86**, 191 (1993).
[20] X. Zianni, P. Butcher, and I. Dharssi, J. Phys.: Condens. Matter **4**, L77 (1992).
[21] C. D. Chen, Solid State Commun. **81**, 785 (1992).
[22] T. Dumelow and S. R. P. Smith, J. Phys.: Condens. Matter **5**, 2919 (1993).
[23] V. M. Agranovich and V. E. Kravtsov, Solid State Commun. **55**, 85 (1985).
[24] T. Dumelow, T. J. Parker, S. R. P. Smith, and D. R. Tilley, Surf. Sci. Rep. **17**, 151 (1993).
[25] F. Bechstedt, H. Gerecke, and H. Grille, Phys. Rev. B **47**, 13 540 (1993).
[26] W. Hayes and R. Loudon, *Scattering of Light by Crystals* (Wiley, New York, 1978).
[27] A. K. Sood, J. Menéndez, M. Cardona, and K. Ploog, Phys. Rev. Lett. **54**, 2111 (1985); **54**, 2115 (1985).
[28] M. P. Chamberlain, M. Cardona, and B. K. Ridley, Phys. Rev. B **48**, 14 356 (1993).
[29] D. Kechrachos, P. R. Briddon, and J. C. Inkson, Phys. Rev. B **44**, 9114 (1991).
[30] R. Hessmer, A. Huber, T. Egeler, M. Haines, G. Tränkle, G. Weimann, and G. Abstreiter, Phys. Rev. B **46**, 4071 (1992).
[31] A. Fainstein, P. Etchegoin, M. P. Chamberlain, M. Cardona, K. Tötemeyer, and K. Eberl, Phys. Rev. B **51**, 14 448 (1995).
[32] M. Haines and G. Scamarcio, in *Phonons in Semiconductor Microstructures*, Vol. 23b of *NATO Advanced Study Institute, Series E: Applied Sciences*, edited by J. P. Leburton *et al.* (Kluwer Academic, The Netherlands, Dordrecht, 1993).
[33] G. Scamarcio, M. Haines, G. Abstreiter, E. Molinari, S. Baroni, A. Fischer, and K. Ploog, Phys. Rev. B **47**, 1483 (1993).
[34] M. Zunke, R. Schorer, G. Abstreiter, W. Klein, G. Weimann, and M. P. Chamberlain, Solid State Commun. **93**, 847 (1995).